



**HAL**  
open science

## Submesoscale Coherent Vortices in the Gulf Stream

Jonathan Gula, Tanya M. Blacic, Robert E. Todd

► **To cite this version:**

Jonathan Gula, Tanya M. Blacic, Robert E. Todd. Submesoscale Coherent Vortices in the Gulf Stream. Geophysical Research Letters, 2019, 46 (5), pp.2704-2714. 10.1029/2019GL081919 . hal-02932212

**HAL Id: hal-02932212**

**<https://hal.science/hal-02932212>**

Submitted on 16 Jun 2022

**HAL** is a multi-disciplinary open access archive for the deposit and dissemination of scientific research documents, whether they are published or not. The documents may come from teaching and research institutions in France or abroad, or from public or private research centers.

L'archive ouverte pluridisciplinaire **HAL**, est destinée au dépôt et à la diffusion de documents scientifiques de niveau recherche, publiés ou non, émanant des établissements d'enseignement et de recherche français ou étrangers, des laboratoires publics ou privés.

Copyright

# Geophysical Research Letters

## RESEARCH LETTER

10.1029/2019GL081919

### Key Points:

- Submesoscale lenses of well-mixed water are observed in seismic reflection images and glider sections across the Gulf Stream
- A realistic numerical simulation is used to characterize these lenses as anticyclonic submesoscale coherent vortices
- Submesoscale coherent vortices are generated where the Gulf Stream interacts with the Charleston Bump

### Supporting Information:

- Supporting Information S1
- Movie S1

### Correspondence to:

J. Gula,  
gula@univ-brest.fr

### Citation:

Gula, J., Blacic, T. M., & Todd, R. E. (2019). Submesoscale coherent vortices in the Gulf Stream. *Geophysical Research Letters*, 46, 2704–2714. <https://doi.org/10.1029/2019GL081919>

Received 12 JAN 2019

Accepted 21 FEB 2019

Accepted article online 27 FEB 2019

Published online 11 MAR 2019

## Submesoscale Coherent Vortices in the Gulf Stream

Jonathan Gula<sup>1</sup> , Tanya M. Blacic<sup>2</sup>, and Robert E. Todd<sup>3</sup> 

<sup>1</sup>Université de Brest, CNRS, IRD, Ifremer, Laboratoire d'Océanographie Physique et Spatiale (LOPS), IUEM, Brest, France, <sup>2</sup>Earth and Environmental Studies, Montclair State University, Montclair, NJ, USA, <sup>3</sup>Department of Physical Oceanography, Woods Hole Oceanographic Institution, Woods Hole, MA, USA

**Abstract** Seismic images and glider sections of the Gulf Stream front along the U.S. eastern seaboard capture deep, lens-shaped submesoscale features. These features have radii of 5–20 km, thicknesses of 150–300 m, and are located at depths greater than 500 m. These are typical signatures of anticyclonic submesoscale coherent vortices. A submesoscale-resolving realistic simulation, which reproduces submesoscale coherent vortices with the same characteristics, is used to analyze their generation mechanism. Submesoscale coherent vortices are primarily generated where the Gulf Stream meets the Charleston Bump, a deep topographic feature, due to the frictional effects and intense mixing in the wake of the topography. These submesoscale coherent vortices can transport waters from the Charleston Bump's thick bottom mixed layer over long distances and spread them within the subtropical gyre. Their net effect on heat and salt distribution remains to be quantified.

**Plain Language Summary** The interior of the ocean is populated by small-scale coherent vortices, which redistribute water properties on the scale of basins. These structures are very difficult to observe. They have no surface signature and small dimensions, on the order of 1–50 km, such that they are missed by satellites and sampled only by chance. Furthermore, climate-scale ocean models do not resolve these type of motions and do not take into account their impacts for the large-scale transport and distribution of heat, nutrients, and other materials. Understanding and parameterizing these phenomena within models is critical for a better prediction of climate. Here we present new observations of submesoscale coherent vortices from seismic images and glider sections in the region of the Gulf Stream. We use a numerical model at very high resolution to reproduce vortices with the same characteristics and to analyze their generation mechanism. These vortices are generated where the Gulf Stream interacts with a deep topographic feature called the Charleston Bump due to frictional effects and intense mixing in the wake of the topography. These vortices transport waters from the Charleston Bump's thick bottom mixed layer and act to spread them all around the subtropical gyre.

## 1. Introduction

Ocean eddies contribute significantly to global fluxes of heat, salt, carbon, and biogeochemical tracers. Surface-intensified mesoscale eddies, with radii typically corresponding to the Rossby deformation radius (30–200 km), have been studied extensively using altimetric observations (Chelton et al., 2007). However, we know much less about the contribution of subsurface eddies, particularly submesoscale (1–30 km) subsurface eddies due to the sparsity of in situ observations able to resolve submesoscales.

Subsurface submesoscale eddies are known as submesoscale coherent vortices (SCVs; McWilliams, 1985) or intrathermocline eddies (Dugan et al., 1982). They are usually defined as energetic eddies with a radius smaller than the Rossby deformation radius, a structure localized in the vertical, and an interior velocity maximum (McWilliams, 1985). SCVs are predominantly anticyclonic with isopycnals forming a convex lens shape (McWilliams, 2016). They can be very long lived (>1 year) and travel far from their origins. As SCVs retain much of their core water mass during their life, they can transport waters with anomalous properties over long distances; for instance, an SCV transporting water from Baja California was sampled near Hawaii (Lukas & Santiago-Mandujano, 2001). The cumulative effect of SCVs can potentially affect the large-scale transport and distribution of heat, nutrients, and other materials.

SCVs have been observed in most regions of the globe (see reviews in Kostianoy & Belkin, 1989; McWilliams, 1985). One of the most well-known types of SCVs are the Meddies formed at the exit of the Mediterranean

Sea (McDowell & Rossby, 1978), which spread salty Mediterranean waters in the subtropical Atlantic Ocean. SCVs also form in eastern boundary regions such as along the West African coast (Kostianoy & Rodionov, 1986a, 1986b). These SCVs are essential for spreading oxygen-poor and nutrient-rich waters into the interior of gyres (Frenger et al., 2018). More generally, SCVs can be generated by interaction of boundary currents with topography, as in the Beaufort Gyre in the Arctic Ocean (D'Asaro, 1988; Manley & Hunkins, 1985), in the Mediterranean Sea along Sardinia (Bosse et al., 2015), at the tail of the Grand Banks (Bower et al., 2013), and over the Mid-Atlantic Ridge (Vic et al., 2018). They also form from wintertime deep convection, as observed in the Labrador Sea (Clarke, 1984; Lilly & Rhines, 2002) and the northwestern Mediterranean Sea (Bosse et al., 2016, 2017; Testor & Gascard, 2003) where they are essential for spreading the newly formed deep waters within ocean basins.

The western part of the North Atlantic Subtropical gyre is a crossroad where many different types of SCVs have been observed. From multiple hydrographic sections in the Sargasso Sea, Dugan et al. (1982) found 19 water lenses between 550- and 800-m depths with thicknesses less than 200 m and diameters less than 65 km. Using an array of current meter moorings deployed for 1 year northeast of Cape Hatteras, Bane et al. (1989) identified 19 SCVs with radii less than 30 km at depths from 900 to 4,000 m. Hydrographic observations during the POLYMODE Local Dynamics Experiment in the Sargasso Sea identified 31 SCVs with quite distinct water mass properties (Lindstrom & Taft, 1986). Based on salinity and oxygen anomalies, McDowell (1986) inferred approximate origins for some of these SCVs: six from the eastern North Atlantic (densities  $26.5 < \sigma < 26.9 \text{ kg/m}^3$ ), three from the Labrador Sea ( $\sigma > 27.8 \text{ kg/m}^3$ ), and others from the Central Sargasso Sea, Antilles, or Gulf Stream. Finally, Ebbesmeyer et al. (1986) found 10 lenses containing seven distinct water masses of the North Atlantic, Mediterranean Sea, and Labrador Sea in the same region; they estimated a spatial density of about 1 lens per  $100 \text{ km}^2$ , which could amount to a total number of 1,000–10,000 lenses in the North Atlantic Ocean.

A number of SCVs observed in the North Atlantic subtropical gyre have unknown generation mechanisms. SCVs made of Mediterranean or Labrador Sea water can be tracked to the Mediterranean outflow and the Labrador Sea water. A few others can be tracked to the West African upwelling, and a number of SCVs in the upper layer of the ocean are likely formed locally by surface processes (convective or wind-driven events). However, the majority of them are formed locally in the subtropical gyre from unknown processes happening below the mixed layer.

SCVs are challenging to detect because of their small horizontal scale. Most observations of SCVs come from hydrographic profiles, and it is difficult to get more than one profile in a given SCV as the horizontal resolution of ship-based hydrographic measurements or Argo float profiles are typically of the same order as the radius of an SCV. Most SCVs do not have a measurable surface expression; only larger mesoscale subsurface eddies can be detected using altimetry (Assassi et al., 2016). Thus, it is difficult to target a specific structure during a field campaign and most observations of SCVs come about by chance. Autonomous underwater gliders have become effective tools to obtain high-spatial-resolution hydrographic data (Rudnick, 2016). They have been able to sample submesoscale vortices on several occasions (Bosse et al., 2016, 2015; Krug et al., 2017; Thomsen et al., 2016). Another available tool for exploring middepth processes is seismic oceanography, which provides two-dimensional vertical snapshots extending down to the seafloor and tens to hundreds of kilometers in length with resolution on the order of meters in the horizontal and vertical. Seismic images can be thought of as maps of the vertical derivative of temperature smoothed by convolution with the seismic source wavelet (Ruddick et al., 2009) with sensitivity down to  $\sim 0.03 \text{ }^\circ\text{C}$  (Nandi et al., 2004). Seismic reflection data have provided images of meddies with unprecedented resolution (Ménèsquen et al., 2012).

Here we present new seismic and glider observations in the western subtropical gyre, which capture submesoscale lenses of well-mixed fluid in the ocean interior. Structures with the same properties are reproduced by a submesoscale-resolving realistic numerical simulation, which is used to study their dynamics and generation mechanism.

## 2. Methods

*Seismic observations.* Seismic data were collected as part of the Eastern North America Margin Community Seismic Experiment in September and October 2014. More than 2,500 km of marine multichannel seismic

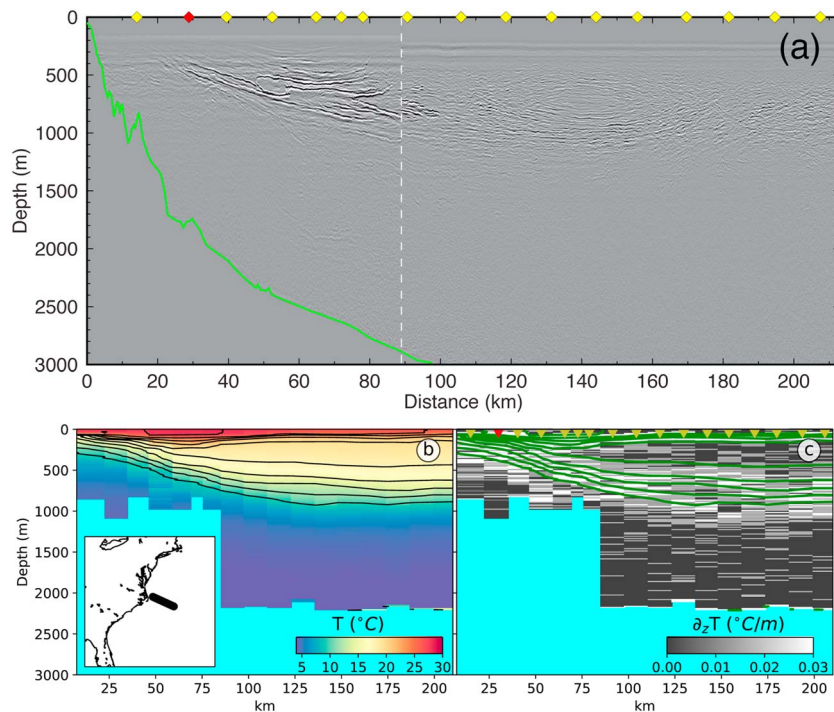


**Figure 1.** Submesoscale lenses in the Gulf Stream front. (a) Seismic image across the Gulf Stream front (see inset in b for location). Yellow (red) diamonds show locations of expendable bathythermograph (conductivity temperature depth) casts. Seafloor is highlighted by a green line. White dashed line denotes transition from Line 1 (eastern portion) to Line 1A (western portion), which was collected after data collection was stopped to repair one of the airgun arrays (time difference at transition between lines is approximately 5 hr). (b) Temperature and (c) vertical gradient of temperature from the expendable bathythermograph and conductivity temperature depth casts along the section.

(MCS) reflection profiles was collected. Several MCS lines crossed the Gulf Stream front, most notably line 1-1A (Figure 1).

MCS data were collected using a standard 2-D source-receiver geometry (Ruddick et al., 2009). The low-frequency (peak frequency of 60-Hz) acoustic source was provided by a 6,600-in.<sup>3</sup> airgun array towed at a depth of 9 m with a shot spacing of 50 m. The reflections were recorded with a 2-ms sampling rate by the R/V *Marcus G. Langseth's* 636-channel, 8-km hydrophone streamer with a 12.5-m hydrophone group spacing resulting in a 6.25-m horizontal sampling interval. During the acquisition of line 1-1A, 16 expendable bathythermographs (XBTs) and one conductivity temperature depth probe (XCTD) were deployed.

Standard MCS data processing routines were followed using the Echos software package by Paradigm. Processing included merging with navigation information, trace editing, suppression of the low-frequency noise band, sorting into common midpoint gathers, band-pass filtering from 8 to 200 Hz, spherical divergence gain, velocity analysis, normal moveout correction, stacking, and time migration. In addition, wavenumber domain poststack filtering was performed.

*Glider observations.* Autonomous underwater gliders have been routinely collecting high-resolution transects across the Gulf Stream since 2015 (Todd, 2017). Steering across measured depth-average currents, the gliders provide profiles of temperature, salinity, and absolute horizontal velocity (Todd et al., 2017) to within a few meters of the seafloor or a maximum depth of 1,000 m with cross-stream resolution of approximately 5 km and temporal spacing of 6 hr or less. Here we focus on a subset of glider observations collected over the Blake Plateau in May–June 2017 during mission 174007.

*Numerical model.* Realistic simulations of the Gulf Stream region at submesoscale-resolving resolution were performed with the Regional Oceanic Modeling System (Shchepetkin & McWilliams, 2005), which solves the free surface, hydrostatic, and primitive equations. The simulation has a horizontal resolution of 500 m and 100 topography-following vertical levels. The model domain spans 1,400 km by 800 km and covers the Gulf Stream along the U.S. continental slope. Boundary conditions are supplied by a sequence of two

lower-resolution simulations that span the entire Gulf Stream region and the Atlantic basin. The simulation is forced by daily winds and diurnally modulated surface fluxes. Vertical mixing of tracers and momentum is done with a K-profile parameterization (Large et al., 1994). The effect of bottom friction is parameterized through a logarithmic law of the wall with a roughness length  $Z_0 = 0.01$  m. The modeling approach is described in detail in Gula et al. (2015a, 2016a), where characteristics of the mean structure and variability of the Gulf Stream in the simulation have been validated against satellite and in situ observations.

### 3. SCVs Near the Gulf Stream

A seismic reflection image spanning the Gulf Stream offshore of Cape Hatteras reveals mesoscale to submesoscale structures at depths of  $\sim 300$ – $1,000$  m (Figure 1a). Striking features are lenses of well-mixed water visible as areas of low reflectivity (little to no coherent reflections) bordered by high-amplitude coherent reflections resulting from large sound speed gradients at the top and bottom of these features. One lens of well-mixed water, with radius around 5 km and thickness of 150 m, is visible 50 km from the coast at 600-m depth. A second lens, with radius around 10 km and thickness of 200 m, is visible 140 km from the coast at 750-m depth.

The seismic reflections result from vertical sound speed gradients that are largely due to temperature gradients on short vertical scales (Sallarès et al., 2009). The coincident transects of temperature  $T$  and vertical temperature gradient  $\partial T/\partial z$  derived from the XBT and XCTD profiles (Figures 1b and 1c) capture vertical structure in the temperature field—including weak  $\partial T/\partial z$  at the location of the lenses—but lack the horizontal resolution necessary to capture the complexity of submesoscale structures at middepths as seen in the seismic image (Figure 1a).

Glider observations near the seaward flank of the Gulf Stream between the Charleston Bump and Cape Hatteras captured a similar submesoscale structure: a lens of well-mixed water centered at 700-m depth with low Brunt-Väisälä frequency  $N^2$  and a thickness of about 300 m (Figure 2). Horizontal velocities at the depth of the lens confirm the presence of anticyclonic rotation (Figure 2b) with local vertical maxima in current speed at depths of 700–800 m (Figure 2d), confirming that the lens is an anticyclonic SCV. The SCV is located between the 26.6- and 27.15- $\text{kg}/\text{m}^3$  isopycnals, which are computed using the potential density anomaly referenced to the surface. Potential density is preferred here to neutral density owing to the difficulty of estimating neutral density in a region close to ocean boundaries with such high spatial and temporal variability and to the minimal differences between the two quantities in the upper 1,000 m of the ocean. In the core of the SCV, waters were anomalously cool (Figure 2c) and fresh (Figure 2f) along isopycnals. This fresh water anomaly indicates that the SCV contained waters within its core that were distinct from surrounding waters. Indeed, the salinity along isopycnals within the core of the SCV matched waters found along the same isopycnals near where those isopycnals intersect the continental slope (along-track distance of approximately 1,500 km in Figures 2c and 2f). This location is adjacent to the Charleston Bump, where strong near-bottom currents flowing over bottom topography result in formation of thick bottom mixed layers (Todd, 2017). It is likely that the observed SCV formed in the lee of the Charleston Bump and then carried well-mixed waters from the generation location in its core.

The structure of the Gulf Stream front in the simulation (Figure 3) is remarkably similar to the observed structure (Figures 1 and 2). A snapshot of the simulation at the location and time of the seismic section qualitatively exhibits the same submesoscale features. Several lenses of well-mixed water with properties consistent with those of observed SCVs are visible offshore of the Gulf Stream front below 500 m. They are associated with anticyclonic relative vorticity  $\zeta = (\nabla \times \mathbf{u}) \cdot \mathbf{z} \approx -0.7f$ , where  $\mathbf{u}$  is the horizontal velocity,  $f$  the Coriolis parameter, and  $\mathbf{z}$  the unit vertical vector. They are also associated with low potential vorticity (PV), which is defined as  $q = \omega_a \cdot \nabla b$ , the dot product of the absolute vorticity  $\omega_a = f\mathbf{z} + \nabla \times \mathbf{u}$  and the gradient of buoyancy  $b = -g \frac{\sigma}{\rho_0}$ , where  $\sigma$  is the potential density referenced to the surface,  $\rho_0$  the mean reference density, and  $g$  the gravitational acceleration.

SCVs with potential densities  $26.5 < \sigma < 27.5$   $\text{kg}/\text{m}^3$  are found regularly in the model (see supporting information Movie S1). Over the 6 months of the simulation, we count about 20 anticyclonic SCVs crossing the cross-Gulf Stream section shown in Figure 3 with radii of 10–25 km and relative vorticity from  $-0.8f$  to  $-0.6f$ . These SCVs are advected by the Gulf Stream and eventually detrained into the Sargasso Sea.

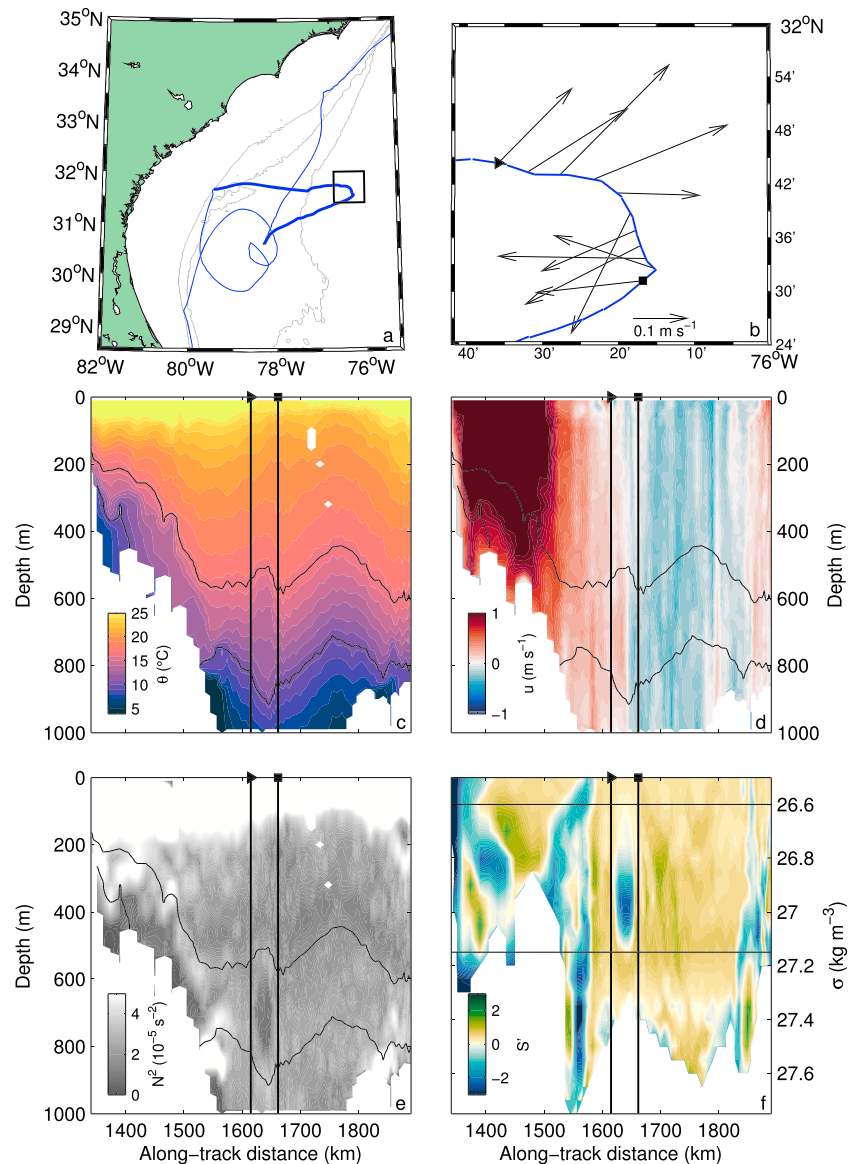


**Figure 2.** Glider observations of a submesoscale coherent vortex adjacent to the Gulf Stream in May–June 2017. (a) Trajectory of the glider in and near the Gulf Stream from central Florida to North Carolina (blue); the bold portion is plotted in subsequent panels. The Charleston Bump is the topographic feature outlined by the 500-m isobath near 31.5°N; the 200- and 1,000-m isobaths are also drawn. (b) Zoomed view of the glider’s trajectory from 25 May (triangle) to 28 May (square) in the box drawn in (a) with horizontal currents vertically averaged between 500 and 900 m. Along-track transects of (c) potential temperature  $\theta$ , (d) eastward velocity  $u$ , and (e) Brunt-Väisälä frequency  $N^2$ . (f) Along-track transect of salinity anomaly  $S'$  along isopycnals normalized by the standard deviation of salinity along each isopycnal. In (c)–(f), the submesoscale coherent vortex is bracketed by the vertical lines and the 26.6- and 27.15-kg/m<sup>3</sup> isopycnals (thin black lines); the vertical lines also bracket the dives for which velocity vectors are shown in (b) with positions denoted by the triangle and square in (b).

The model probably underestimates the number of SCVs in this region, in particular, SCVs from remote origins, which may not be simulated correctly in the coarser parent simulations or may not have enough time to reach this region from their generation site.

#### 4. Generation of SCVs

Mechanisms of anticyclonic SCV formation must account for the creation of low PV anomalies; that is, they must provide a spatially or temporally intermittent source of low PV (McWilliams, 1985). The impermeability theorem states that there is no net transport of PV across isopycnal surfaces (Haynes & McIntyre, 1987).

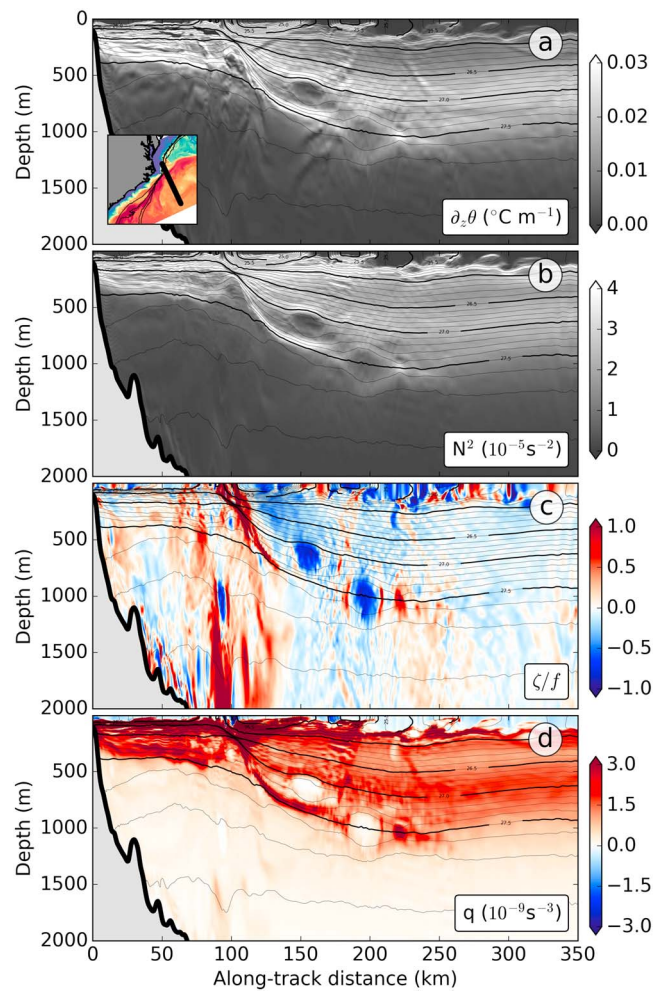


**Figure 3.** Submesoscale coherent vortices in a high-resolution model of the Gulf Stream. Vertical sections across the Gulf Stream front in the simulation east of Cape Hatteras (location shown in the upper panel insert) showing (a) potential temperature vertical gradient  $\partial\theta/\partial z$  ( $^{\circ}\text{C}/\text{m}$ ), (b) Brunt-Väisälä frequency  $N^2$ , (c) relative vorticity  $\zeta$  (normalized by  $f$ ), and (d) potential vorticity  $q$  ( $\text{s}^{-3}$ ). Potential density is shown in black contours on all panels.

An SCV observed within a layer bounded by two given isopycnal surfaces has to be associated with nonconservative or diabatic effects within the same layer of fluid. There is no creation or destruction of PV within a layer bounded by two isopycnal surfaces away from boundaries, but PV can still be concentrated or diluted in the presence of interior nonconservative or diabatic effects. However, the values of PV found in SCVs are so extreme compared to the background PV that they most likely originate from regions where isopycnal surfaces intersect a boundary (i.e., the ocean's surface or bottom) in the presence of strong frictional or diabatic effects. At the surface, the diabatic and frictional effects can result from convective (Marshall & Schott, 1999) or wind-driven destruction of PV (Thomas, 2008). At the bottom, they can result from geothermal forcing (Baker et al., 1987), mixing (McWilliams, 1985), and bottom friction (D'Asaro, 1988).

Frictional effects at the bottom can trigger the following sequence of events: strong generation of relative vorticity in the boundary layer, separation from the slope, violent instability, strong mixing, and formation of SCVs (Molemaker et al., 2015; McWilliams, 2016). Recent high-resolution realistic simulations have shown that this mechanism might be ubiquitous (Gula et al., 2015b, 2016b; Molemaker et al., 2015; Vic et al., 2015). If a current is flowing in the direction of Kelvin wave propagation (with the topography on its right in the Northern Hemisphere), then the PV is reduced in the bottom boundary layer (Benthuisen & Thomas, 2012), centrifugal instability can be triggered, and anticyclonic SCVs may form (D'Asaro, 1988; Gula et al., 2016b; Molemaker et al., 2015). On the other hand, if a current is flowing in the direction opposite to the Kelvin wave

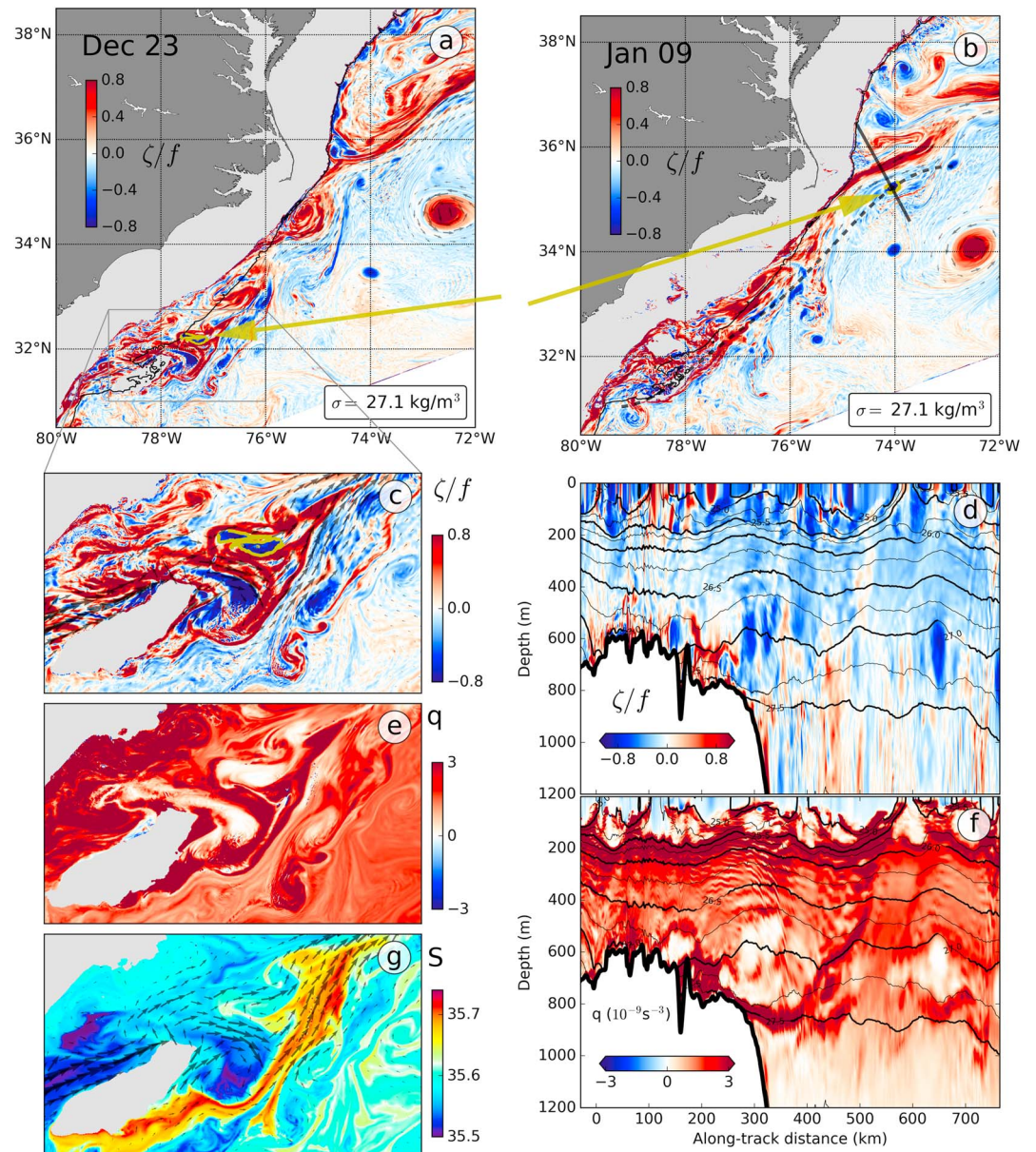


**Figure 4.** Generation of submesoscale coherent vortices (SCVs) in the lee of the Charleston Bump. (a, b) Snapshots of the relative vorticity  $\zeta$  (normalized by  $f$ ) on the  $27.1\text{-kg/m}^3$  isopycnal: (a) shortly after the generation of several SCVs and (b) at the time of Figure 3. Yellow contours and arrows in panels (a)–(c) indicate the location of the water masses forming the core of the SCV shown in Figure 3; 600-m isobath is shown in black. The plain line in panel (b) shows the location of the section shown in Figure 3. (c, e, and g) Zooms of panel (a) showing relative vorticity, potential vorticity ( $\text{s}^{-3}$ ), and salinity. (d) Relative vorticity and (f) potential vorticity in the along-stream direction (shown as a dashed gray line in panel b) at the time of panel (b). Black contours showing potential density are repeated on panels (d) and (f).

propagation direction, positive PV is generated, horizontal shear instability can be triggered, and cyclonic SCVs may form (Gula et al., 2015b; Krug et al., 2017).

SCVs found east of the Gulf Stream front in the model (Figure 3) are in the density range  $26.9\text{--}27.6 \text{ kg/m}^3$ . These isopycnals do not outcrop at the surface in the model, but they intersect the bottom along the continental slope of the southeastern United States (e.g., Figure 4). The Gulf Stream flows along the continental margin with the slope on its left, so it tends to generate positive vorticity. However, the Charleston Bump acts as an island in the Gulf Stream and allows isopycnals to intersect the sea floor on either side (Figure 4a). Thus, the flow interacts with it intermittently to generate relative vorticity and PV of both signs (Figures 4c–4f). The anticyclonic SCVs visible in the wake of the Charleston Bump east of the Gulf Stream



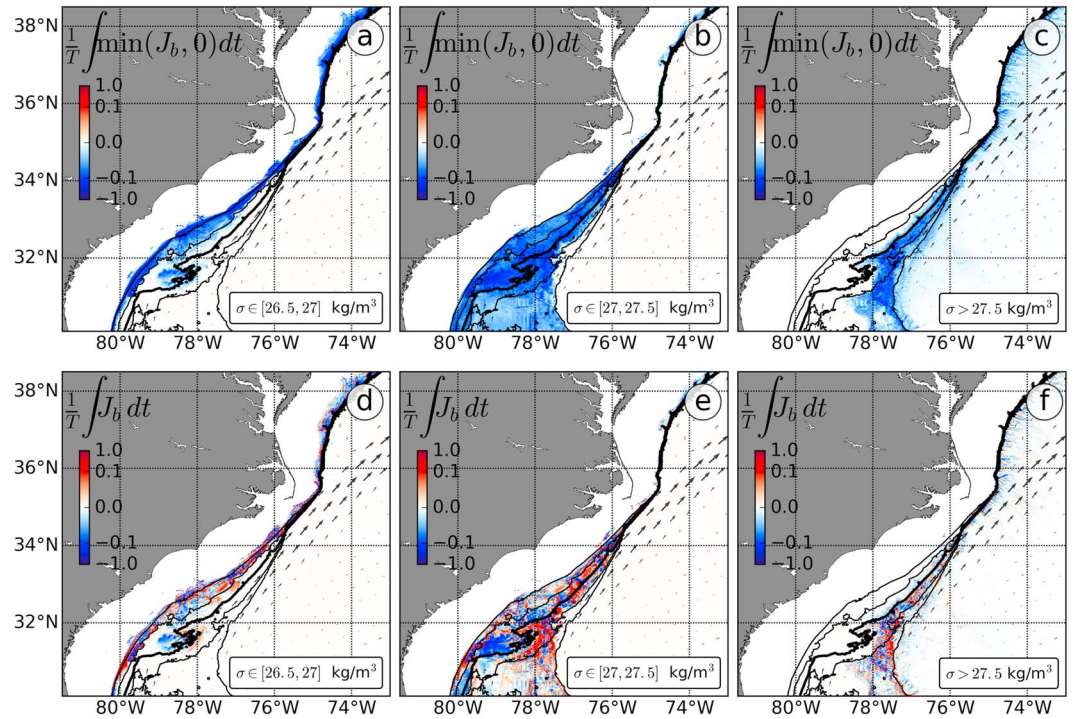


**Figure 5.** Bottom injection of potential vorticity (PV). (top) Conditional integral for negative bottom PV fluxes only and (bottom) total bottom PV fluxes averaged over 6 months between isopycnals 26.5–27 kg/m<sup>3</sup> (left), 27–27.5 kg/m<sup>3</sup> (middle), and denser than 27.5 kg/m<sup>3</sup> (right). Arrows show the mean velocity field on the 27-kg/m<sup>3</sup> isopycnal.

cyclonic front in Figures 3 and 4b all originate from current-topography interactions at the location of the Bump (see supporting information Movie S1).

The water on the shoreward side of the bump is cooler and fresher than the water offshore along a given isopycnal. As anticyclonic vorticity is generated where the stream flows with the bump on its right, the nascent anticyclonic SCVs entrain preferentially anomalously cool and fresh water from the shoreward side (Figure 4g).

A conservation equation for PV ( $q$ ) can be written using a flux form:

$$\frac{\partial q}{\partial t} + \nabla \cdot \left[ \underbrace{q\mathbf{u}}_{J_A} - \underbrace{\omega_a \frac{Db}{Dt}}_{J_D} + \underbrace{\nabla b \times \mathbf{F}}_{J_F} \right] = 0, \quad (1)$$

where  $\mathbf{F}$  represents the nonconservative forces per unit mass (Marshall et al., 2001). The advection of PV is  $J_A$ , the diabatic flux of PV is  $J_D$ , and the frictional flux of PV is  $J_F$ . When integrated over a volume defined by two isopycnal surfaces that each intersect the seafloor but do not outcrop at the surface, the equation reduces to the following:

$$\frac{\partial}{\partial t} \int q dV = \int -(J_D + J_F) dA = \int J_b dA, \quad (2)$$

where  $\mathcal{A}$  represents the bottom area delimited by the two isopycnal surfaces and  $J_b = -(J_D + J_F)$ . This equation means that PV substance within an isopycnal layer can change only due to diabatic and/or frictional processes over the area  $\mathcal{A}$ .

This provides a convenient diagnostic to locate regions where injection of negative PV and creation of anticyclonic SCVs are more likely over a given density range. To highlight such regions, we conditionally average instantaneous negative PV fluxes over the duration  $T$  of the simulation ( $1/T \int \min(J_b, 0) dt$ , Figures 5a–5c) and compute mean PV fluxes ( $1/T \int J_b dt$ , Figures 5d–5f) over several density ranges. The Charleston Bump is the location where most of the negative PV is generated for potential densities between

26.5 and 27.5 kg/m<sup>3</sup>. In particular, mean PV fluxes are negative in the region of the bump between the 400- and 600-m isobaths (Figures 5a and 5b). Negative PV generation is also possible all along the continental slope between 26.5 and 27 kg/m<sup>3</sup> in regions shallower than 500 m. South of the Gulf Stream separation point at Cape Hatteras, negative PV generation along the slope will most likely be due to the presence of recurrent cyclonic eddies on the cyclonic side of the Gulf Stream, which induce local reversals of the current but are less likely to form long-lived coherent structures due to the strong shear of the current (Gula et al., 2016a). North of the separation point, negative PV generation happens more consistently as the time mean flow is equatorward. SCVs with potential densities less than 27.5 kg/m<sup>3</sup> are routinely formed there, but they cannot easily cross the North Wall of the Gulf Stream due to its strong positive PV anomaly and are often sheared apart when they reach it (Figure 4a). SCVs with potential densities greater than 27.5 kg/m<sup>3</sup> are created due to interactions between the southward deep western boundary current and the continental slope (one example is visible in Figure 3c). These SCVs have properties similar to those generated along the Grand Banks (Bower et al., 2013) and are deep enough to cross the Gulf Stream without being destroyed.

## 5. Conclusions

New observations of SCVs are reported in the western North Atlantic subtropical gyre. Seismic images of the Gulf Stream front capture submesoscale lens-shaped features at depths greater than 500 m. A glider section captures a similar feature adjacent to the Gulf Stream and downstream of the Charleston Bump. These features have radii of 5–20 km and thicknesses of 150–300 m, typical signatures of anticyclonic SCVs. Submesoscale-resolving simulations for the Gulf Stream region using Regional Oceanic Modeling System reproduce SCVs with the same size and depth as those observed. The SCVs are generated primarily where the Gulf Stream meets the Charleston Bump due to frictional effects and intense mixing in the wake of the topography.

Riser et al. (1986) examined a similar SCV in the Sargasso Sea using observations from the POLYMODE Local Dynamics Experiment; the 20-km-wide SCV was 300 m thick and centered at 750 m. Its core salinity of 35.42 ppt at a potential density of 27.05 kg/m<sup>3</sup> was consistent with waters regularly observed near the Charleston Bump, as well as waters much farther south as suggested by Riser et al. (1986). Given the similarity to the SCVs examined here, it seems likely that the SCV studied by Riser et al. (1986) was generated near the Charleston Bump by the processes described here.

Observations and models provide glimpses of the ocean interior richness and suggest that it is populated by a large number of deep submesoscale structures, which may be essential to redistribute water properties. However, the ocean is still largely undersampled and observational data remains limited. Thus, a global census of SCVs and their impact on global circulation is still lacking.

## References

- Assassi, C., Morel, Y., Vandermeersch, F., Chaigneau, A., Pegliasco, C., Morrow, R., et al. (2016). An index to distinguish surface- and subsurface-intensified vortices from surface observations. *Journal of Physical Oceanography*, 46(8), 2529–2552. <https://doi.org/10.1175/JPO-D-15-0122.1>
- Baker, E. T., Massoth, G. J., & Feely, R. A. (1987). Cataclysmic hydrothermal venting on the Juan de Fuca Ridge. *Nature*, 329, 149–151. <https://doi.org/10.1038/329149a0>
- Bane, J. M., O'Keefe, L. M., & Watts, D. R. (1989). Mesoscale eddies and submesoscale, coherent vortices: Their existence near and interactions with the Gulf Stream. In J. C. J. Nihoul & B. M. Jamart (Eds.), *Mesoscale/synoptic coherent structures in geophysical turbulence, Elsevier Oceanography Series* (Vol. 50, pp. 501–518). Amsterdam: Elsevier. [https://doi.org/10.1016/S0422-9894\(08\)70204-6](https://doi.org/10.1016/S0422-9894(08)70204-6)
- Benthuisen, J., & Thomas, L. N. (2012). Friction and diapycnal mixing at a slope: Boundary control of potential vorticity. *Journal of Physical Oceanography*, 42, 1509–1523.
- Bosse, A., Testor, P., Houpert, L., Damien, P., Prieur, L., Hayes, D., et al. (2016). Scales and dynamics of submesoscale coherent vortices formed by deep convection in the northwestern Mediterranean Sea. *Journal of Geophysical Research: Oceans*, 121, 7716–7742. <https://doi.org/10.1002/2016JC012144>
- Bosse, A., Testor, P., Mayot, N., Prieur, L., D'Ortenzio, F., Mortier, L., et al. (2017). A submesoscale coherent vortex in the Ligurian Sea: From dynamical barriers to biological implications. *Journal of Geophysical Research: Oceans*, 122, 6196–6217. <https://doi.org/10.1002/2016JC012634>
- Bosse, A., Testor, P., Mortier, L., Prieur, L., Taillandier, V., d'Ortenzio, F., & Coppola, L. (2015). Spreading of Levantine Intermediate Waters by submesoscale coherent vortices in the northwestern Mediterranean Sea as observed with gliders. *Journal of Geophysical Research: Oceans*, 120, 1599–1622. <https://doi.org/10.1002/2014JC010263>
- Bower, A. S., Hendry, R. M., Amrhein, D. E., & Lilly, J. M. (2013). Direct observations of formation and propagation of subpolar eddies into the Subtropical North Atlantic. *Deep-Sea Research*, 85, 15–41.
- Chelton, D. B., Schlax, M. G., Samelson, R. M., & de Szoeke, R. A. (2007). Global observations of large oceanic eddies. *Geophysical Research Letters*, 34, L15606. <https://doi.org/10.1029/2007GL030812>

### Acknowledgments

J. G. gratefully acknowledges support from the French government, managed by the French National Agency for Research (ANR), through programs ISblue (ANR-17-EURE-0015) and LabexMER (ANR-10-LABX-19) and from LEFE/IMAGO through the project AO2017-994457-RADII. Simulations were performed using HPC resources from GENCI-TGCC (grant 2017-A0010107638). Simulations output is available upon request. Seismic data were processed using the Echos software package by Paradigm, Matlab, and Generic Mapping Tools. The Eastern North America Margin Community Seismic Experiment was funded by the National Science Foundation under grant OCE-1347498 and UNOLS; cruise data are freely available via the Marine Geoscience Data System Academic Seismic Portal at Lamont-Doherty Earth Observatory (<http://www.marine-geo.org/portals/seismic/>). Spray glider observations in the Gulf Stream are available from <http://spraydata.ucsd.edu> and should be cited using the following DOI (10.21238/S8SPRAY2675; Todd & Owens, 2016). Spray glider operations were funded by the National Science Foundation (OCE-1633911) and the Office of Naval Research (N000141713040).

- Clarke, R. A. (1984). Transport through the Cape Farewell-Flemish Cap section. *Rapports et procès-verbaux des réunions - Conseil international pour l'exploration de la mer*, 185, 120–130.
- D'Asaro, E. A. (1988). Generation of submesoscale vortices: A new mechanism. *Journal of Geophysical Research*, 93(C6), 6685–6693.
- Dugan, J. P., Mied, R. P., Mignerey, P. C., & Schuetz, A. F. (1982). Compact, intrathermocline eddies in the Sargasso Sea. *Journal of Geophysical Research*, 87(C1), 385–393. <https://doi.org/10.1029/JC087iC01p00385>
- Ebbesmeyer, C. C., Taft, B. A., McWilliams, J. C., Shen, C. Y., Riser, S. C., Rossby, H. T., et al. (1986). Detection, structure and origin of extreme anomalies in a Western Atlantic oceanographic section. *Journal of Physical Oceanography*, 16, 591–612.
- Frenger, I., Bianchi, D., Stührenberg, C., Oschlies, A., Dunne, J., Deutsch, C., et al. (2018). Biogeochemical role of subsurface coherent eddies in the ocean: Tracer cannonballs, hypoxic storms, and microbial stewpots? *Global Biogeochemical Cycles*, 32(2), 226–249. <https://doi.org/10.1002/2017GB005743>
- Gula, J., Molemaker, M. J., & McWilliams, J. C. (2015a). Gulf Stream dynamics along the Southeastern U.S. Seaboard. *Journal of Physical Oceanography*, 45(3), 690–715.
- Gula, J., Molemaker, M. J., & McWilliams, J. C. (2015b). Topographic vorticity generation, submesoscale instability and vortex street formation in the Gulf Stream. *Geophysical Research Letters*, 42, 4054–4062. <https://doi.org/10.1002/2015GL063731>
- Gula, J., Molemaker, M. J., & McWilliams, J. C. (2016a). Submesoscale dynamics of a Gulf Stream frontal eddy in the South Atlantic Bight. *Journal of Physical Oceanography*, 46, 305–325.
- Gula, J., Molemaker, M. J., & McWilliams, J. C. (2016b). Topographic generation of submesoscale centrifugal instability and energy dissipation. *Nature Communications*, 7, 12811. <https://doi.org/10.1038/ncomms12811>
- Haynes, P. H., & McIntyre, M. E. (1987). On the evolution of vorticity and potential vorticity in the presence of diabatic heating and frictional or other forces. *Journal of the Atmospheric Sciences*, 44(5), 828–841. [https://doi.org/10.1175/1520-0469\(1987\)044h0828:OTEOVAi2.0.CO;2](https://doi.org/10.1175/1520-0469(1987)044h0828:OTEOVAi2.0.CO;2)
- Kostianoy, A. G., & Belkin, I. M. (1989). A survey of observations on intrathermocline eddies in the world ocean. In J. C. J. Nihoul & B. M. Jamart (Eds.), *Mesoscale/synoptic coherent structures in geophysical turbulence, Elsevier Oceanography Series* (Vol. 50, pp. 821–841). Amsterdam: Elsevier. [https://doi.org/10.1016/S0422-9894\(08\)70223-X](https://doi.org/10.1016/S0422-9894(08)70223-X)
- Kostianoy, A. G., & Rodionov, V. B. (1986a). *Intrathermocline eddies in the ocean*, pp. 50–52. Moscow (in Russian): P.P. Shirshov Inst. of Oceanology.
- Kostianoy, A. G., & Rodionov, V. B. (1986b). On the formation of intrathermocline eddies in the Canary upwelling region. *Okeanologiya (in Russian)*, 26, 892–895.
- Krug, M. J., Swart, S., & Gula, J. (2017). Submesoscale cyclones in the Agulhas Current. *Geophysical Research Letters*, 44, 346–354. <https://doi.org/10.1002/2016GL071006>
- Large, W. G., McWilliams, J. C., & Doney, S. (1994). Oceanic vertical mixing: A review and a model with a nonlocal boundary layer parameterization. *Reviews of Geophysics*, 32, 363–403.
- Lilly, J. M., & Rhines, P. B. (2002). Coherent eddies in the Labrador Sea observed from a mooring. *Journal of Physical Oceanography*, 32(2), 585–598. [https://doi.org/10.1175/1520-0485\(2002\)032h0585:CEITLSi2.0.CO;2](https://doi.org/10.1175/1520-0485(2002)032h0585:CEITLSi2.0.CO;2)
- Lindstrom, E. J., & Taft, B. A. (1986). Small water property transporting eddies: Statistical outliers in the hydrographic data of the POLYMODE Local Dynamics Experiment. *Journal of Physical Oceanography*, 16, 613–631.
- Lukas, R., & Santiago-Mandujano, F. (2001). Extreme water mass anomaly observed in the Hawaii ocean time-series. *Geophysical Research Letters*, 28(15), 2931–2934. <https://doi.org/10.1029/2001GL013099>
- Manley, T. O., & Hunkins, K. (1985). Mesoscale eddies of the Arctic Ocean. *Journal of Geophysical Research*, 90(C3), 4911–4930. <https://doi.org/10.1029/JC090iC03p04911>
- Marshall, J., Jamous, D., & Nilsson, J. (2001). Entry, flux, and exit of potential vorticity in ocean circulation. *Journal of Physical Oceanography*, 31, 777–789.
- Marshall, J., & Schott, F. (1999). Open-ocean convection: Observations, theory, and models. *Reviews of Geophysics*, 37, 1–64.
- McDowell, S. E. (1986). On the origin of eddies discovered during the POLYMODE Local Dynamics Experiment. *Journal of Physical Oceanography*, 16, 632–652.
- McDowell, S. E., & Rossby, H. T. (1978). Mediterranean water: An intense mesoscale eddy off the bahamas. *Science*, 202, 1085–1087.
- McWilliams, J. C. (1985). Submesoscale, coherent vortices in the ocean. *Reviews of Geophysics*, 23, 165–182.
- McWilliams, J. C. (2016). Submesoscale currents in the ocean. *Proceedings of the Royal Society A*, 472(2189), 20160117. <https://doi.org/10.1098/rspa.2016.0117>
- Ménesguen, C., Hua, B. L., Carton, X., Klingelhoefer, F., Schnürle, P., & Reichert, C. (2012). Arms winding around a meddy seen in seismic reflection data close to the Morocco coastline. *Geophysical Research Letters*, 39, L05604. <https://doi.org/10.1029/2011GL050798>
- Molemaker, M. J., McWilliams, J. C., & Dewar, W. K. (2015). Submesoscale instability and generation of mesoscale anticyclones near a separation of the California Undercurrent. *Journal of Physical Oceanography*, 45, 613–629.
- Nandi, P., Holbrook, W. S., Pearse, S., Páramo, P., & Schmitt, R. W. (2004). Seismic reflection imaging of water mass boundaries in the Norwegian Sea. *Geophysical Research Letters*, 31, L23311. <https://doi.org/10.1029/2004GL021325>
- Riser, S. C., Owens, W. B., Rossby, H. T., & Ebbesmeyer, C. C. (1986). The structure, dynamics, and origin of a small-scale lens of water in the Western North Atlantic thermocline. *Journal of Physical Oceanography*, 16(3), 572–590. [https://doi.org/10.1175/1520-0485\(1986\)016h0572:TSDAOOi2.0.CO;2](https://doi.org/10.1175/1520-0485(1986)016h0572:TSDAOOi2.0.CO;2)
- Ruddick, B., Song, H., Dong, C., & Pinheiro, L. (2009). Water column seismic images as maps of temperature gradient. *Oceanography*, 22, 192–205. <https://doi.org/10.5670/oceanog.2009.19>
- Rudnick, D. L. (2016). Ocean research enabled by underwater gliders. *Annual Review of Marine Science*, 8(1), 519–541. <https://doi.org/10.1146/annurev-marine-122414-033913>
- Sallarès, V., Biescas, B., Buffett, G., Carbonell, R., Dañoibeitia, J. J., & Pelegrí, J. L. (2009). Relative contribution of temperature and salinity to ocean acoustic reflectivity. *Geophysical Research Letters*, 36, L00D06. <https://doi.org/10.1029/2009GL040187>
- Shchepetkin, A. F., & McWilliams, J. C. (2005). The Regional Oceanic Modeling System (ROMS): A split-explicit, free-surface, topography-following-coordinate ocean model. *Ocean Modelling*, 9, 347–404.
- Testor, P., & Gascard, J.-C. (2003). Large-scale spreading of deep waters in the western Mediterranean Sea by submesoscale coherent eddies. *Journal of Physical Oceanography*, 33(1), 75–87. [https://doi.org/10.1175/1520-0485\(2003\)033h0075:LSSODWi2.0.CO;2](https://doi.org/10.1175/1520-0485(2003)033h0075:LSSODWi2.0.CO;2)
- Thomas, L. N. (2008). Formation of intrathermocline eddies at ocean fronts by wind-driven destruction of potential vorticity. *Dynamics of Atmospheres and Oceans*, 45(3–4), 252–273. <https://doi.org/10.1016/j.dynatmoce.2008.02.002>
- Thomsen, S., Kanzow, T., Krahnmann, G., Greatbatch, R. J., Dengler, M., & Lavik, G. (2016). The formation of a subsurface anticyclonic eddy in the Peru-Chile Undercurrent and its impact on the near-coastal salinity, oxygen, and nutrient distributions. *Journal of Geophysical Research: Oceans*, 121, 476–501. <https://doi.org/10.1002/2015JC010878>

- Todd, R. E. (2017). High-frequency internal waves and thick bottom mixed layers observed by gliders in the Gulf Stream. *Geophysical Research Letters*, *44*, 6316–6325. <https://doi.org/10.1002/2017GL072580>
- Todd, R. E., & Owens, W. B. (2016). Gliders in the Gulf Stream. Scripps Institution of Oceanography, Instrument Development Group, Publicly available dataset. <https://doi.org/10.21238/S8SPRAY2675>
- Todd, R. E., Rudnick, D. L., Sherman, J. T., Owens, W. B., & George, L. (2017). Absolute velocity estimates from autonomous underwater gliders equipped with Doppler current profilers. *Journal of Atmospheric and Oceanic Technology*, *34*(2), 309–333. <https://doi.org/10.1175/JTECH-D-16-0156.1>
- Vic, C., Gula, J., Roulet, G., & Pradillon, F. (2018). Dispersion of deep-sea hydrothermal vent effluents and larvae by submesoscale and tidal currents. *Deep-Sea Research Part I*, *133*, 1–18. <https://doi.org/10.1016/j.dsr.2018.01.001>
- Vic, C., Roulet, G., Carton, X., Capet, X., Molemaker, M. J., & Gula, J. (2015). Eddy-topography interactions and the fate of the Persian Gulf Outflow. *Journal of Geophysical Research: Oceans*, *120*, 6700–6717. <https://doi.org/10.1002/2015JC011033>